



HAL
open science

Supramolecular architectures of mononuclear nickel(II) and homobinuclear copper(II) complexes square with the 5,5'-dimethyl-2,2'-bipyridine ligand: Syntheses, Crystal structures and Hirshfeld surface analyses

Wassim Maalej, Rim Jaballi, Asma Ben Rached, Philippe Guionneau, Nathalie Daro, Zakaria Elaoud

► To cite this version:

Wassim Maalej, Rim Jaballi, Asma Ben Rached, Philippe Guionneau, Nathalie Daro, et al.. Supramolecular architectures of mononuclear nickel(II) and homobinuclear copper(II) complexes square with the 5,5'-dimethyl-2,2'-bipyridine ligand: Syntheses, Crystal structures and Hirshfeld surface analyses. *Journal of Molecular Structure*, 2022, 150 (Part 2), 131728 (16 p.). 10.1016/j.molstruc.2021.131728 . hal-03425004

HAL Id: hal-03425004

<https://hal.science/hal-03425004>

Submitted on 10 Nov 2021

HAL is a multi-disciplinary open access archive for the deposit and dissemination of scientific research documents, whether they are published or not. The documents may come from teaching and research institutions in France or abroad, or from public or private research centers.

L'archive ouverte pluridisciplinaire **HAL**, est destinée au dépôt et à la diffusion de documents scientifiques de niveau recherche, publiés ou non, émanant des établissements d'enseignement et de recherche français ou étrangers, des laboratoires publics ou privés.

Supramolecular architectures of mononuclear nickel(II) and homobinuclear copper(II) complexes square with the 5,5'-dimethyl-2,2'-bipyridine ligand: Syntheses, Crystal structures and Hirshfeld surface analyses.

Wassim Maalej,^{*a} Rim Jaballi,^a Asma Ben Rached,^a Philippe Guionneau,^b Nathalie Daro^b and Zakaria Elaoud^a

Two new compounds based on one mononuclear nickel(II) and one homobinuclear copper(II) complexes respectively and of general formula $[\text{Ni}(\text{dmbpy})_2(\text{CH}_3\text{COO})]\text{ClO}_4$ (1) and $[\text{Cu}_2(\text{dmbpy})_4(\text{CH}_3\text{COO})_3]\text{ClO}_4$ (2) with dmbpy = 5,5'-dimethyl-2,2'-bipyridine, were synthesized by hydrothermal treatment. Both were influenced by the coordinated acetate ion molecule. The crystal and molecular structures of (1) and (2) were determined by single crystal X-ray diffraction method and both compounds were additionally characterized by means of elemental and thermogravimetric analysis, FT-IR spectroscopy, powder X-ray diffraction and UV-visible. The mononuclear complex (1) shows a distorted octahedral geometry around the metal ion. On the other hand, the copper(II) compound crystallizes as an homobinuclear system, in which each of the metal ions is located into the N_2O_3 coordination spheres adopting a distorted square pyramidal geometry. In (2) the intramolecular distance between two copper atoms is of the order of $\text{Cu1-Cu2} = 3.38$ (2) Å. In both crystal packing of these two complexes, H-bonding, $\pi\cdots\pi$, and C-H $\cdots\pi$ interactions are operative in forming supramolecular motifs. Complex (1) displays two 1-D chains that lead to form $R_g^8(42)$ ring motifs, repetition of which generates a 2-D supramolecular network. These chains interact with the neighbouring ones via intermolecular C-H $\cdots\pi$ and $\pi\cdots\pi$ stacking interactions, leading to the formation of a 3D-stacking network (2-D+1-D \rightarrow 3-D). Formation of a 2-D supramolecular sheet in the solid state structure of (2) is facilitated by the C-H $\cdots\text{O}$, C-H $\cdots\pi$ and $\pi\cdots\pi$ interactions (1-D+1-D \rightarrow 2-D). Hirshfeld surface analysis and theoretical calculations were carried out on the two compounds. The results clearly show that C-H $\cdots\text{O}$, C-H $\cdots\pi$ and $\pi\cdots\pi$ stacking interactions play a paramount role in the stabilization of the supramolecular architecture of (1) and (2). In addition, adsorption spectra reveal their semiconductive nature (4.19 eV for 1 and 4.43 eV for 2).

Introduction

The structural chemistry of organometallic architectures continues to attract interest from scientists in crystal engineering, mainly due to the development of new phenomena and the potential applications of the resultant materials.¹⁻⁶ In supramolecular chemistry, in addition to the coordinate covalent bonding, hydrogen bonds are effective in establishing particular contacts which occur regularly, and play a significant and repetitive role in directing molecules during crystallization.⁷⁻¹⁰ In this way, the interactions, such as hydrogen bonding and $\pi\cdots\pi$ stacking, may serve as additional forces sustaining the coordination networks, or as the forces interlinking discrete or low-dimensional coordination motifs into higher-dimensional architectures organic-inorganic hybrid

materials. Among the non-covalent interactions, H-bonding is the most widely used synthons over other and can able to generate hybrid compounds, which are more elastic in nature. Among the other types of non-covalent interactions, $\pi\cdots\pi$ stacking between the aromatic rings are used in construction of hybrid compounds.¹¹⁻¹⁵ The characteristic features of these materials are the exceptional electrical and optical properties.¹⁶⁻²³ Moreover, a large number of studies showed that post-synthetic functionalization or direct syntheses with ligands having suitable functionality can impart hydrogen bond capabilities to the organic-inorganic hybrid.^{24,25} Besides, one of the most widely studied functional groups that have been used to impart hydrogen bonding capabilities to the hybrid is the amino, carbonyl, anhydride, cyano group, etc.,²⁶⁻³⁰ Even more recently, the self-assembly processes are sensitive to diverse synthetic conditions in some cases, change of reaction conditions such as the solvent, pH and temperature for a given set of organic ligands and metal ions can cause various supramolecular architectures.^{31,32} In this regard, solvent molecules or counter-ions (CH_3COO^- , NO_3^- , NO_2^- , ClO_4^- , etc) may also dramatically influence the overall solid-state architecture

^a Laboratory of Physical and Chemistry of Solid State, University of Sfax, Faculty of Sciences of Sfax, B.P. 1171, 3000 Sfax, Tunisia.

^b CNRS, Univ. Bordeaux, Bordeaux INP, ICMCB, UMR 5026, 87 avenue Dr A. Schweitzer, 33608 Pessac, France.

† Corresponding author, E-mail: maalej_wassim@hayoo.fr
maalej.wassim@fsg.rnu.tn.

ARTICLE

by participating in metal coordination and hydrogen bonding. On the basis of the aforementioned thoughts and as an expansion of our research on supramolecular architectures of the 5,5'-dimethyl-2,2'-bipyridine based salts, in which aromatic N play a key vital role in generating three-dimensional (3D) networks through $\pi \dots \pi$ stacking interaction.³³ In the present work, we report the synthesis, spectroscopic characterization and X-ray crystal structures of two new Ni(II) and Cu(II) coordination complexes as well as a deep analysis of their interesting crystalline architectures formed by supramolecular interactions.

Experimental

General Procedures

The starting compounds including the 5,5'-dimethyl-2,2'-bipyridine ligand, the nickel and copper perchlorate salts and the solvents were purchased from commercial suppliers (Sigma-Aldrich, Merck and others). All chemical reagents were used without further purification. Deionized water, acetonitrile and acetic acid was used as solvent in this work. C, H, and N microanalyses were carried out with a Perkin-Elmer system 2000 elemental analyzer and scanning electron microscopy (SEM). Infrared spectra (IR) was recorded on a PerkinElmer Spectrum TM 100 FT-IR spectrometer as KBr pellets in the range 4000–400 cm^{-1} . Differential thermal analysis (DTA) and thermogravimetric analysis (TGA) measurements were performed on our heating the sample in a platinum crucible from 300 to 700 K in a SETARAM thermal analyser (TG-ATD92) under air at a heating rate of 5 K min^{-1} . The UV–vis diffuse reflectance spectrum was measured at room temperature using a Shimadzu-type 3101 PC UV spectrophotometer equipped with a double beam monochromator covering the spectrum range from 200 nm to 1000 nm. Powder X-ray diffraction patterns (PXRD) were recorded using a PANalytical X'Pert Pro diffractometer ($\text{Cu K}\alpha_1$, 1.5406 Å) and the Single crystal X-ray diffraction (SCXRD) data collection were run using an Apex-II Bruker diffractometer.

Synthesis of $[\text{Ni}(\text{dmbpy})_2(\text{CH}_3\text{COO})]\text{ClO}_4$ (1)

A mixture of 5,5'-dimethyl-2,2'-bipyridine (10 mmol, 1.84 g) and nickel (II) perchlorate hexahydrate (5 mmol, 1.28 g) were dissolved in 35 ml of H_2O (1.5 ml), MeCN (10 ml) and AcOH (10 ml) to give a blue solution. The mixture was then introduced into a 125 ml autoclave, which was sealed and heated under autogenous pressure at 130°C for 72 h. After cooling to room temperature the products, shiny blue crystals were washed with distilled water, ethanol, and acetone followed by drying in air. Elemental analysis (%) calcd: C, 53.32; H, 4.61; N, 9.56. Found: C, 52.26; H, 3.79; N, 9.18.

Synthesis of $[\text{Cu}_2(\text{dmbpy})_4(\text{CH}_3\text{COO})_3]\text{ClO}_4$ (2)

The compound (2) was prepared by the hydrothermal treatment of a mixture of 5,5'-dimethyl-2,2'-bipyridine (10 mmol, 1.84 g), copper (II) perchlorate hexahydrate (5 mmol,

1.31 g), H_2O (1.5 ml), MeCN (10 ml) and AcOH (10 ml) were placed in Teflon-lined stainless steel vessel. The sample was heated at 130°C for 3 days and then cooled to room temperature. After washed by ethanol, and acetone, light yellow crystals were obtained with a yield of 45 % based on Cu. Elemental analysis (%) calcd: C, 46.66; H, 4.27; N, 7.25. Found: C, 45.21; H, 3.37; N, 6.94. The reaction scheme followed for the synthesis of Ni(II) and Cu(II) complexes is shown in Fig. 1.

PXRD was used to demonstrate the phase purity of nickel(II) and copper(II) complexes. As shown in Fig. 2, the experimental PXRD patterns of complexes are well-matched with the calculated patterns obtained from their single crystal data, demonstrating the phase purity of complexes.

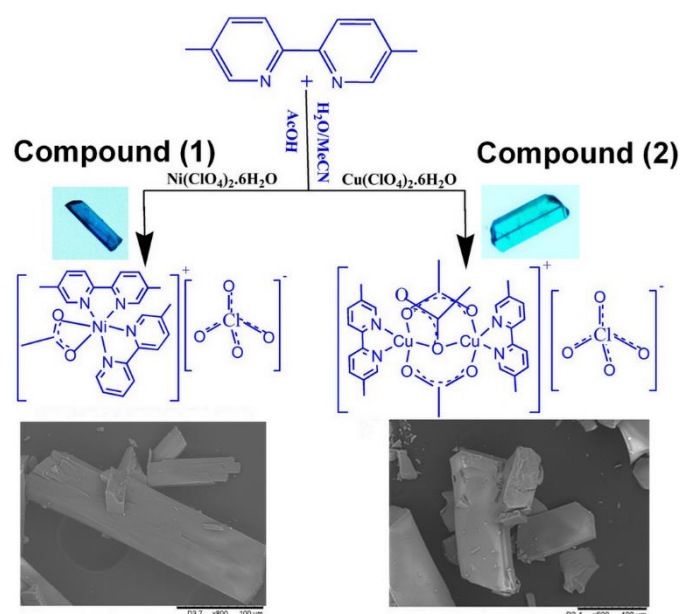


FIG. 1 Chemical scheme and single-crystals morphologies for (1) and (2).

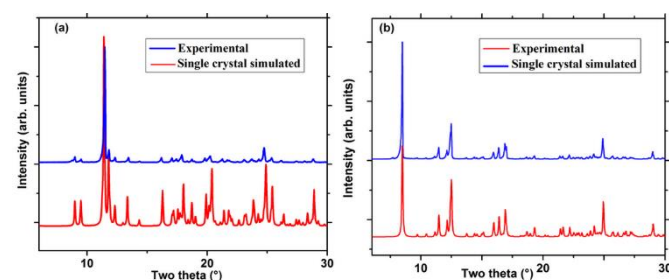


FIG. 2 X-ray diffraction patterns obtained directly from the experiment for the powder (blue) and derived from the single-crystal analysis (red) for (1) and (2).

IR spectra of the complexes

FT-IR spectra of the two compounds are similar (Fig. S1) and the absorption bands can be assigned on the basis of the literature. Several main peaks were detected, due to functional group vibrations. In all cases, a series of weak peaks in the region ca. 3700–2940 cm^{-1} were observed, corresponding to C–H stretching vibrations of the aromatic ring and C–H alkyl (methyl) group.³⁴ In the complexes (1) and (2), the strong absorption

bands in the region 1550–1600 cm^{-1} corresponds to $\nu(\text{COO})_{\text{sym}}$ frequency, respectively, are associated to the acetate ligand. At lower frequency range, the bands observed at 1240 in (1) and 1301 cm^{-1} in (2) can be ascribed are (COO) symmetric deformation modes.^{35,36} The bands in the range 1673–1413 cm^{-1} are characteristics for the skeletal vibrations of the aromatic rings. The (dmbpy) ligand has some characteristic vibrational bands of the $\nu(\text{C}=\text{C})$ and $\nu(\text{C}=\text{N})$ groups at 1650 1430 cm^{-1} , respectively.^{37,38} The C-H in-plane bending and C-H out-of-plane bending vibrations sort out in the range of 1410–1150 cm^{-1} and 820–660 cm^{-1} respectively.³⁷ Furthermore, the presence of bands at 1093, 1039, 834 and 616 cm^{-1} for complex (1) and the bands at 1080, 1046, 842 and 626 cm^{-1} in complex (2), indicate a T_d symmetry of ClO_4^- , suggest the presence of perchlorate ion outside the coordination sphere.^{39–41} Finally, the coordination of ligands is substantiated by a band in the range 540–421 cm^{-1} for all of the complexes corresponding to M-O and M-N stretching vibrations.^{42,43}

Thermogravimetric analysis

To estimate the stability of the coordination compounds, thermogravimetric analysis (TGA) and differential thermogravimetric analysis (DTA) were carried out. As shown in Fig. S2, the thermogram of mononuclear nickel (1) indicates the stability of the compound up to 549 K but the homobinuclear copper compound (2) shows the decomposition in 520 K. The Cu(II) complex exhibits single decomposition stage at the temperature range of 500–650 K which corresponds to the removal of one 5,5'-dimethyl-2,2'-bipyridine and two acetate moieties, are related by exothermic effect in 550 K (found 39.54%, calculated 39.14%) Fig. S3. In the case of nickel complex, the TG curve shows that the complex exhibits the continuous weight loss because another reaction starts before the one of decomposition reactions ends in the temperature

range of 520–840 K. Therefore, it is difficult to distinguish the reactions from each other. The total weight loss in this temperature range is 62.42% corresponds to the removal of one 5,5'-dimethyl-2,2'-bipyridine and 1 acetate and 1 perchlorate moieties (calculated 58.51%), with three exothermic peaks observed on the DTA curve at 620.65, 678.69 and 740.06 K.

X-ray crystal structure determination

Suitable single crystals of complexes (1) and (2) were mounted on a APEX-II Bruker diffractometer equipped with a graphite-monochromated Mo- K_α radiation ($\lambda = 0.71073 \text{ \AA}$) at 298 K. All absorption corrections were performed using the SADABS program. The two structures were solved by the direct methods and refined by full-matrix least-squares fitting on F^2 by SHELXTL-97⁴⁴ through the WinGX program suite.⁴⁵ All non-hydrogen atoms were refined with anisotropic thermal parameters. Hydrogen atoms were located at geometrically calculated positions and treated by a mixture of independent and constrained refinement. Crystallographic data and structural refinements for compounds Ni and Cu are summarized in Table 1. The selected bond lengths parameters of the compounds 1 and 2 are summarized in Tables S1 and S2, respectively.

Hirshfeld surface analysis

Known to be very efficient to describe the intermolecular contact in molecular crystals, notably in view of structure-properties relationships,^{46,47} Hirshfeld surfaces⁴⁸ were generated using Crystal Explorer 17.5 based on the results from X-ray studies. Directions and strengths of intermolecular interactions within the crystal were mapped onto the Hirshfeld surfaces using the descriptor d_{norm} , which is a ratio encompassing the distances of any surface point to the nearby interior d_i (the distance from a point on the surface to the nearest atom inside the surface) and exterior d_e (the distance

Table 1 Crystallographic data and details of refinements for complexes 1 and 2

Identification code	(1)	(2)
formula	$[\text{Ni}(\text{dmbpy})_2(\text{CH}_3\text{COO})]\text{ClO}_4$	$[\text{Cu}_2(\text{dmbpy})_4(\text{CH}_3\text{COO})_3]\text{ClO}_4$
Mr (g.mol ⁻¹)	583.68	772.14
Crystal system	Triclinic	Triclinic
Space group	P-1	P-1
a (Å)	8.6159 (3)	8.019 (5)
b (Å)	10.8313 (3)	11.557 (5)
c (Å)	15.8252 (4)	18.735 (6)
α (°)	98.300 (8)	76.096 (7)
β (°)	102.502 (8)	86.625 (7)
γ (°)	110.712 (9)	73.857 (8)
Volume(Å ³)	1308.57 (11)	1618.9 (13)
Z-space group	2	2
F (000)	303	396
σ_{calc} (mg m ⁻³)	1.486	1.584
μ (mm ⁻¹)	0.89	1.46
Data/restraints/params	2634/0/344	7456/0/424
GOF on F ²	1.19	1.10
R ₁ (I = 2 σ (I))	0.052	0.084
ωR_2 (all data)	0.114	0.241
w	$=1/[\sigma^2(\text{Fo}^2)+0.0334\text{P}^2]+2.9081\text{P}$ where $\text{P} = (\text{Fo}^2 + 2\text{Fc}^2)/3$	$=1/[\sigma^2(\text{Fo}^2)+0.0477\text{P}^2]+24.2284\text{P}$ where $\text{P} = (\text{Fo}^2 + 2\text{Fc}^2)/3$
$\Delta\rho_{\text{max}}, \Delta\rho_{\text{min}}$ (e Å ⁻³)	0.36/−0.42	1.67/−1.63
CCDC no.	2085397	2085398

ARTICLE

from a point on the surface to the nearest atom outside the surface) atoms and the van der Waals radii of the atoms, given by the equation (1). Associated plots of d_i vs. d_e , referred to as fingerprint plots (FP), are given, which are useful in identifying and comparing different kinds of interactions.⁴⁹ The value of d_{norm} is negative (red colour) or positive (blue colour) when intermolecular contacts are shorter or longer than van der Waals separations, respectively. Additionally, the combination of d_i and d_e in the form of a 2D fingerprint plot^{50,51} provides summary of intermolecular contacts in the crystal. 2D FP are considered unique for a molecule in a given molecular environment, hence shapes, area and symmetry of those plots can be used for an assessment and comparison of supramolecular properties of related molecules.

$$d_{norm} = \frac{d_i - r_i^{vdw}}{r_i^{vdw}} + \frac{d_e - r_e^{vdw}}{r_e^{vdw}} \quad eq (1)$$

Results and discussion

Crystal structures of complex $[\text{Ni}(\text{dmbpy})_2(\text{CH}_3\text{COO})]\text{ClO}_4$ (**1**)

The single crystal X-ray diffraction results indicate that (**1**) crystallizes in the triclinic space group P-1 consisting of one Ni(II) ions, two (dmbpy) ligands, one acetate ion and one isolated ClO_4^- tetrahedral. The asymmetric unit of (**1**) is shown in Fig. 3. The Ni ion is six-coordinated in a distorted octahedral coordination sphere, including four N atoms (Ni-N1 = 2.053 (5) Å, Ni-N2 = 2.047 (4) Å, Ni-N3 = 2.059 (4) Å, Ni-N4 = 2.064 (4) Å) from two (dmbpy) ligands as well as two oxygen atoms (Ni-O1 = 2.104 (3) Å, Ni-O2 = 2.115 (4) Å) coming from one CH_3COO^- ion. The cisoid and transoid bond angles fall in the regions 62.6(1) - 102.6(2)° and 162.3(2) - 177.5 (2)°, respectively, indicating the octahedral coordination to be distorted. The isolated ClO_4^- tetrahedra are slightly distorted and exhibit a range of 109.0 (3) - 110.2 (3)° for the O-Cl-O angles, with an average Cl-O distance of 1.436 (10) Å.

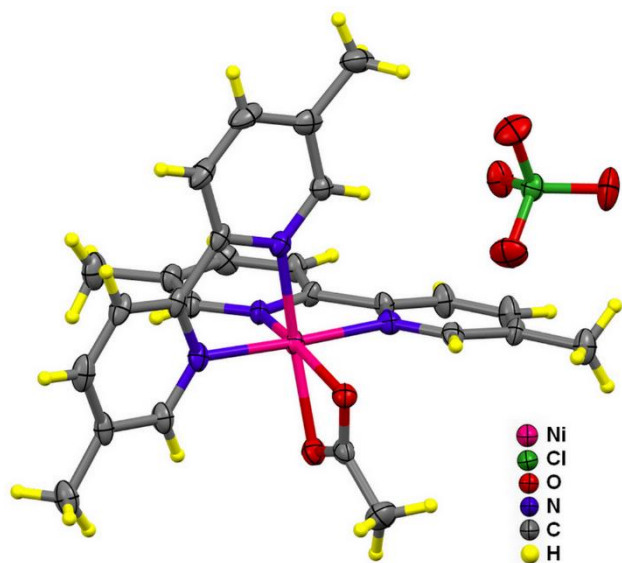


Fig. 3 ORTEP view of the asymmetric unit of **1** with displacement ellipsoid at 50% probability.

In the absence of chemical entities capable of establishing strong H-bonding, the molecules are assembled solely by a combination of weak C-H...O and intramolecular π - π stackings. The oxygen atom (O1) of the acetate anion are the strongest hydrogen bond acceptors and aromatic C-halogen groups are the strongest H bond donors in the system. However, the most significant hydrogen bond interaction is the intermolecular hydrogen bonds observed between C7...H with O1' [C7...O1 = 3.194 (6) Å, H7...O1 = 2.33 (1) Å, C7-H7...O1 = 155 (1)°] which leads to the formation of the centrosymmetric a hydrogen bonded dimer with Ni(1)...Ni(1) (1-x, 1-y, 1-z) separation of 7.429(3) Å (Fig. 4a). The hydrogen bonded ring motifs, in the formalism of graph-set analysis of hydrogen-bond patterns,⁵² that are found for $[\text{Ni}(\text{dmbpy})_2(\text{CH}_3\text{COO})]^+$ are the $S_1^1(5)$ and the common $R_2^2(12)$ motifs consisting of 12 atoms, with 2 donors and 2 acceptor (Fig. 4b).

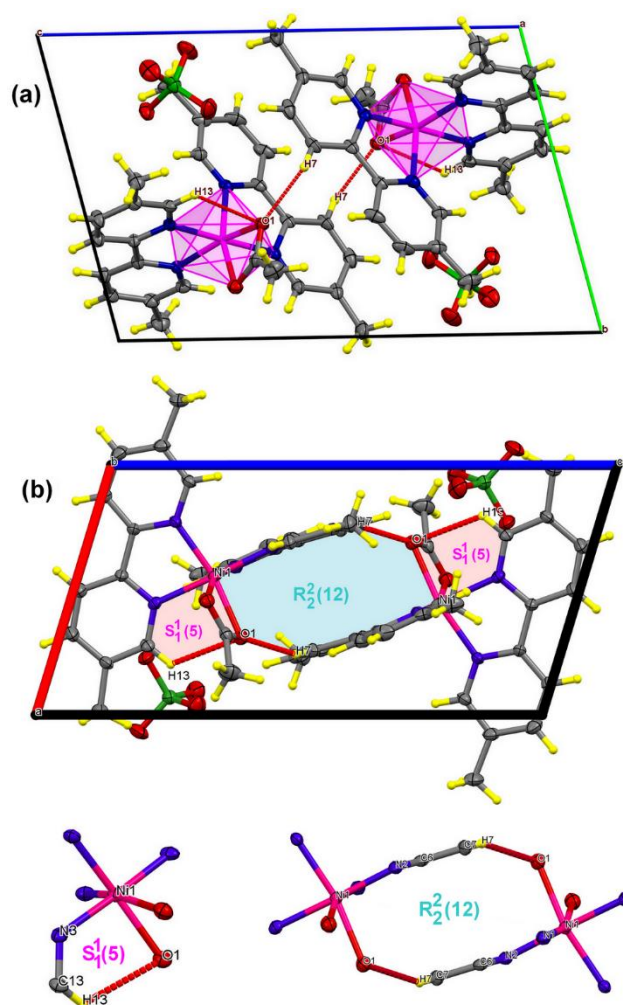


Fig. 4 (a) Crystal packing of the molecules in **1** projected onto the (011) plane, and detail of the hydrogen bonding showing the centrosymmetric dimers (thermal ellipsoids represent 50% probability). (b) The hydrogen-bonding motif in the (101) plane.

On the other hand, the perchlorate anions are also involved in H-bonding. the three oxygen atoms, namely O3, O4 and O6 of the ClO_4^- moiety, There are five C-H...O interactions between non-coordinated oxygen atoms of the perchlorate groups as acceptor and

aromatic (H1, H16, H19 and H26A) hydrogens. These distances are all well below the sum of the van der Waals radii, i.e. 2.72 Å for hydrogen and oxygen.⁵³ Moreover, the structure of (1) consists of the perchlorate anions connected to neighbouring dimeric $R_2^2(12)$ ring motif units by weak, C16/C19–H...O6 hydrogen bonds, therefore generating a centrosymmetric $R_4^4(18)$ dimeric ring centred at $(\frac{1}{2}, \frac{1}{2}, 0)$ (Fig. 5a) leading to one-dimensional (1D) parallel chains along [001] direction with the Ni1...Ni1 distance of 9.93 Å (Fig. 5b). In (dmbpy) ligand, the carbon atom C(26) acts as donor to the perchlorate oxygen atom O3ⁱⁱⁱ [symmetry code: (iii) x, y–1, z] to form another infinite chain along [010] direction (Fig. 6a). The combination of these two 1-D chains leads to form $R_8^8(42)$ ring motif, repetition of which gives a 2-D supramolecular network in the (011) plane (Fig. 6b).

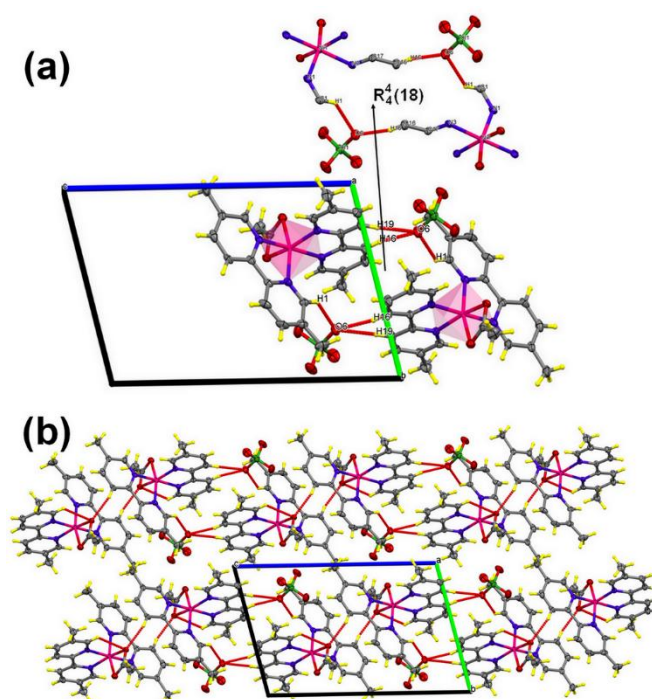


Fig. 5 (a) C-H...O6 hydrogen bonds (red lines) for **1** showing $R_4^4(18)$ the graph-set motif. (b) Formation of 1D tape in complex **1** through association of $[Ni(dmbpy)_2(CH_3COO)]ClO_4$ through C-H...O1 hydrogen bonds.

Despite the large number of aromatic rings within the crystal packing, only two intermolecular $\pi\cdots\pi$ and two C–H... π short contacts have been detected, probably due to the separating action of the intervening chloride ions. For aromatic ligand, $\pi\cdots\pi$ interaction appear (Cg1...Cg2 = 3.775 Å) (Fig. 7a). There also exist C–H... π interactions between the C23–H23B and C24–H24C bond of methyl (dmbpy) ligand and the centroid of the phenyl ring with the separation distance of 3.080 Å (C23...Cg4) and 3.406 Å (C24...Cg3), respectively (Fig. 7b). In addition, the perchlorate anion which interacts with the 5,5'-dimethyl-2,2'-bipyridine ring through anion... π interaction further interacts with the oxygen atoms (O3 and O6) of ClO_4^- group, which plays an important role in stabilizing this structure (Fig. 7c). The shortest separation distance reflecting this interaction is O6...Cg3 = 3.581 Å, which is included of the range (3.3–3.8 Å).⁵⁴

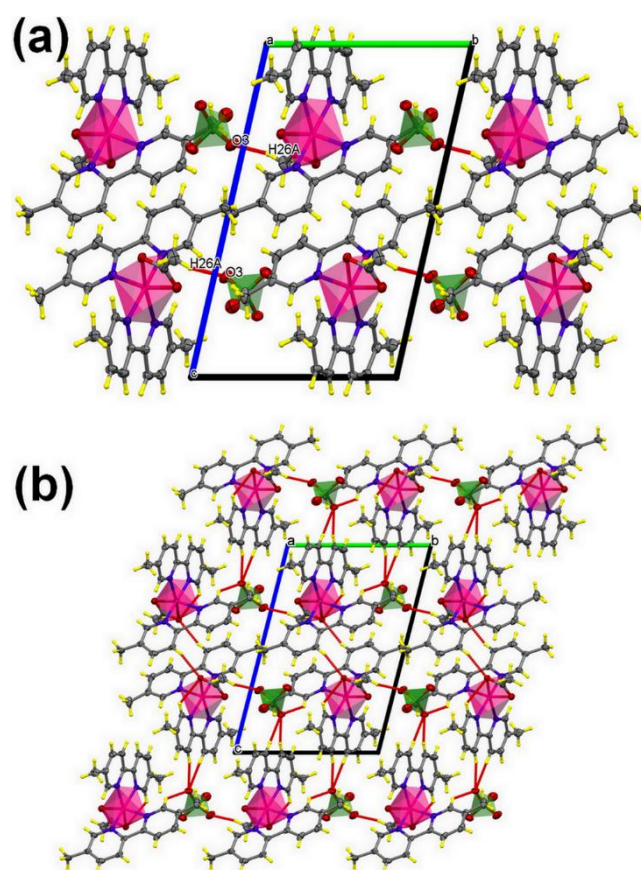


Fig. 6 The C–H...O3 interactions (a) The infinite 1D helix chain along b axis in **1** (b) The illustration of the 2D layer of **1** in the bc plane.

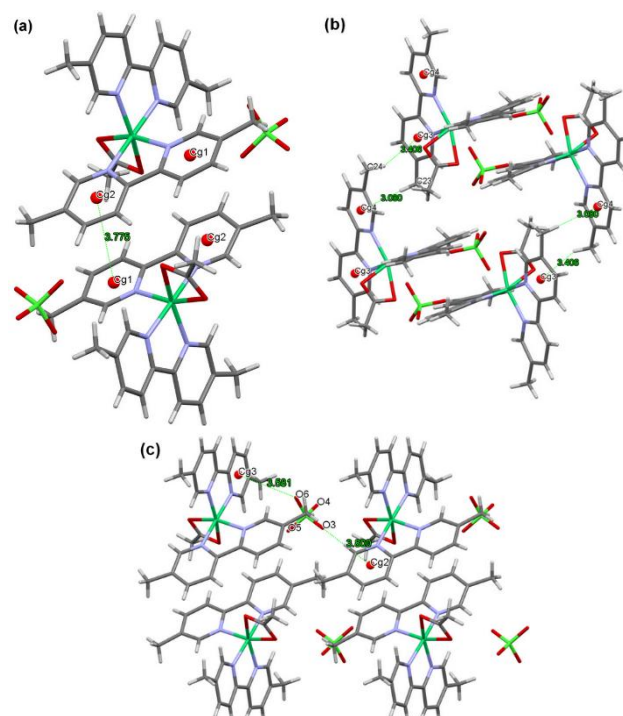


Fig. 7 (a) A view of the $\pi\cdots\pi$ stacking for compound **1**. (b) A view of the C–H... π interactions in **1** (c) The formation of the O... π interactions by cations and ClO_4^- for compound **1**.

ARTICLE

Thus anion $\cdots\pi$ interaction together form a chain zig-zag of non-covalent interactions which stabilize the 3D supramolecular network of $[\text{Ni}(\text{dmbpy})_2(\text{CH}_3\text{COO})]\text{ClO}_4$, as shown in Fig. 8. The geometrical parameters of these intermolecular interactions are collected in Table 1.

Table 2 Hydrogen bond, C-H $\cdots\pi$ and $\pi\cdots\pi$ stacking interactions in 1.

D-H \cdots A ^{a,b}	D-H/Å	H \cdots A/Å	D \cdots A/Å	\angle D-H \cdots A/ $^\circ$
C13—H13 \cdots O1	0.93	2.54	3.077 (6)	117
C7—H7 \cdots O1 ⁱ	0.93	2.33	3.194 (6)	155
C26—H26A \cdots O3 ⁱⁱⁱ	0.96	2.50	3.347 (7)	147
C19—H19 \cdots O4 ⁱⁱ	0.93	2.65	3.319 (6)	130
C1—H1 \cdots O6	0.93	2.62	3.386 (7)	139
C16—H16 \cdots O6 ⁱⁱ	0.93	2.33	3.244 (6)	169
C19—H19 \cdots O6 ⁱⁱ	0.93	2.44	3.366 (6)	173

^aSymmetry codes: (i) $-x+1, -y+1, -z+1$; (ii) $-x+1, -y+1, -z$; (iii) $x, y-1, z$

$\pi\cdots\pi$ interactions, Cg \cdots Cg distance

Cg1 ^{iv} \cdots Cg2	3.775(3)
--------------------------------	----------

^bSymmetry codes: (iv) $1-x, 1-y, 1-z$

^b Cg1 and Cg2 are the centroids of the N1-C1-C2- C3-C4-C5, N2-C6-C7- C8-C9-C10,

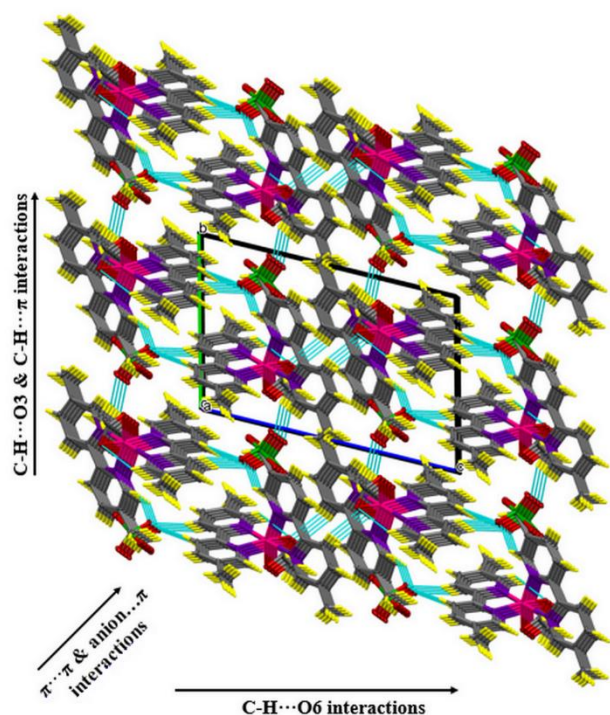


Fig. 8 3D supramolecular structure induced by intermolecular interactions in 1 complex.

Crystal structures of complex $[\text{Cu}_2(\text{dmbpy})_4(\text{CH}_3\text{COO})_3]\text{ClO}_4$ (2)

In order to understand the details of the crystal structure of (2), single-crystal X-ray diffraction data were collected at 293 K. The analyses indicate that (2) crystallizes in the triclinic crystal system with the space group P-1. The molecular structure of copper (II)

complex consists of homobinuclear $[\text{Cu}_2(\text{dmbpy})_4(\text{CH}_3\text{COO})_3]^+$ complex cations that is balanced by ClO_4^- counter ions. The molecular structure of (2) is shown in Fig. 9a, selected bond lengths and angles are given in Table S2. Each copper atom is surrounded by a 5.5'-dmbpy bidentate ligand through two N-donor atoms and three acetate groups coordinated differently to copper ions; two bidentate groups (CH_3COO^-) are linked to two Cu^{2+} ions via four oxygen atoms [$\text{Cu1-O1} = 1.932$ (6) Å, $\text{Cu2-O2} = 1.942$ (6) Å, $\text{Cu1-O3} = 1.950$ (6) Å and $\text{Cu2-O4} = 2.217$ (6) Å], and a third monodentate group is coordinated with the two copper ions only by the oxygen atom [$\text{Cu1-O5} = 2.172$ (5) Å and $\text{Cu2-O5} = 1.992$ (5) Å]. The O5 atom acts as a bridge between the two copper ions (Cu1 and Cu2). It occupies an axial position of the intermediate geometry of Cu1 and an equatorial position in the pyramidal environment with a square base of Cu2. The axial Cu2–O4 bond parameter is 2.217 (6) Å. The four short Cu–N bond lengths are in the range from 1.999 (6) to 2.030 (6) Å. These results are comparable to those found for similar compounds.⁵⁵ Within this structure, each copper ion is in a five-coordinated CuN_2O_3 environment with geometries swing between the ideal square pyramidal and trigonal bipyramidal structures, this is justified by the trigonal parameter τ , $\tau = (\beta - \alpha)/60$: where α and β are the largest angles around the Cu^{2+} ion. We noticed that $\tau = 1$ corresponds to a trigonal bipyramidal geometry and $\tau = 0$ to a square pyramidal geometry. As regard to the Cu1 center, the value of $\tau = 0.47$, indicating that its geometry is intermediate between the ideal square pyramidal and trigonal bipyramidal prisms.⁵⁶ The geometric parameters of the coordination sphere of Cu1 are collected in Table S2, revealing an axial elongation of the intermediate along the direction Cu \cdots O5. The axial distance Cu1–O5 is longer than the other equatorial bonds Cu–O1, O2, N3, N4 (Fig. 9éb). In addition, the values of the angles N/O–Cu1–O/N are ranged between 80.3 (3) and 169.1 (2) $^\circ$.

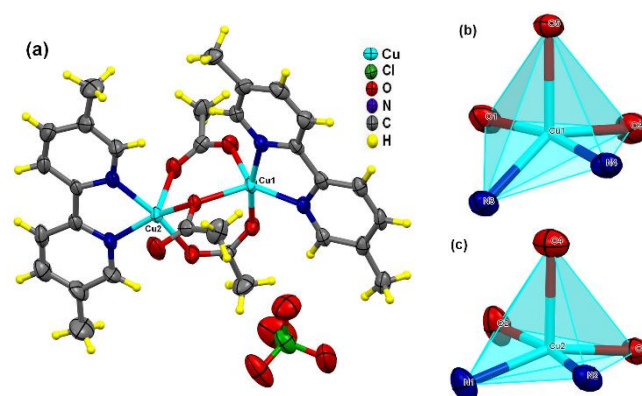


Fig. 9 (a) ORTEP view of the asymmetric unit of 2 with displacement ellipsoid at 50% probability. Cu1O3N2 (a) and Cu2O3N2 (b) square pyramidal formed by the oxygen atoms from four two bidentate acetate ligands completed by one monodentate acetate oxygen and two (dmbpy) nitrogen atom for Cu1 and Cu2, respectively.

These results indicate that the Jahn-Teller effect is involved in the coordination sphere of the copper Cu1 center which the environment is described as a geometric ranging from the square pyramidal to the trigonal bipyramidal structure. The second copper ion is surrounded in the equatorial plane by the atoms O2, O5, N1

and N2 (Fig. 9c). The value of $\tau = 0.20$, this value highlights the presence of a square pyramidal geometry. The cisoid and transoid bond angles fall in the regions 80.6 (3)–101.7 (3)° and 157.4 (3)–169.7 (3)°, respectively, indicating the distorted SP geometry. This can be justified by the Jahn–Teller effect, which is engaged in the coordination sphere of copper (4 + 1). The deviations from the least-squares plane through the CuN_2O_2 atoms in Cu1 and Cu2 are 0.418 and 0.236 respectively. The distance between two copper is of the order of $\text{Cu1–Cu2} = 3.38$ (2) Å. This distance is shorter than binuclear Cu (II) complexes.⁵⁷ This value of the intermetallic distance will prompt us to think about studying the magnetic properties of this material.⁵⁸

The crystal structure of (2) reveals that the crystal packing of the polymorphs are stabilized through different hydrogen bonding interactions. Given that the lack of acidic protons on the (dmbpy) ligands and acetate anion, no classical hydrogen bond interaction is expected to play a prominent role in the crystal packing. However, several kinds of weak hydrogen bonds involving the carbon bound hydrogen atoms are observed in compound 2. Consequently, two weak $\text{C13–H13}\cdots\text{O1}$ (3.227 (3) Å) and $\text{C1–H1}\cdots\text{O2}$ (2.914 (10) Å) hydrogen bonds are found between the (dmbpy) ligand and the (CH_3COO^-) anion, forming an intramolecular bond with the motif $\text{S}_1^1(5)$. In addition, the C4 atom, which belongs to the $[\text{Cu}_2(\text{dmbpy})_4(\text{CH}_3\text{COO})_3]^+$ cation acts as a hydrogen bond donor to O4 atom of acetate group forming a centrosymmetric a hydrogen bonded $\text{R}_2^2(12)$ dimeric ring centred at $(\frac{1}{2}, 0, \frac{1}{2})$, with $\text{Cu(1)}\cdots\text{Cu(1)}$ and $\text{Cu(2)}\cdots\text{Cu(2)}$ separation of 13.235 (4) Å and 7.501(2) Å, respectively (Fig. 10a). Furthermore, the two C19 and C30 carbon atoms acts as donor to the perchlorate oxygen atom O7 in the molecule, so generating centrosymmetric a $\text{R}_4^4(20)$ dimeric ring centred at $(\frac{1}{2}, \frac{1}{2}, 0)$, with $\text{Cu(1)}\cdots\text{Cu(1)} = 9.316$ (6) Å (Fig. 10b). The combination of two types of $\text{R}_2^2(12)$ and $\text{R}_4^4(20)$ ring motif leads to the formation of one-dimensional (1D) parallel chains are arranged

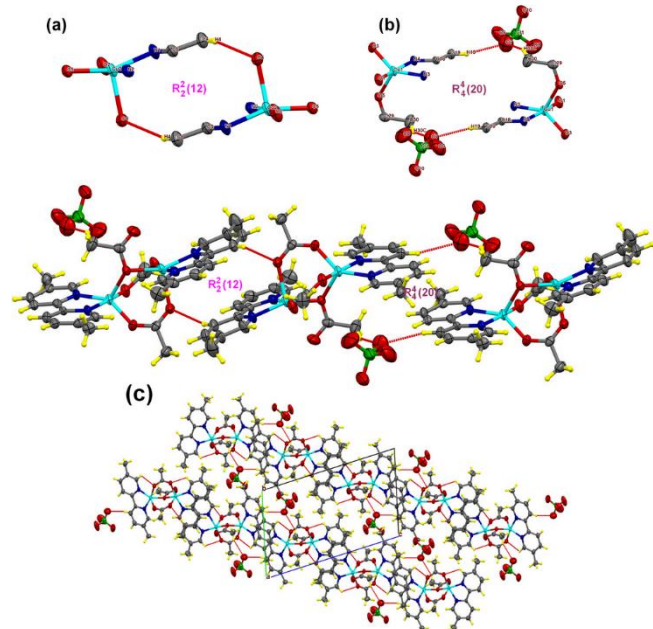


Fig. 10 The hydrogen-bonding motif for compound 2 (a) $\text{R}_2^2(12)$ ring motif (b) $\text{R}_4^4(20)$ ring motif. (c) View of the 1D supramolecular chain by intermolecular C–H \cdots O in 2.

into sheets lying parallel to the crystallographic bc diagonal. (Fig. 10c). Such types of hydrogen bonds have already been investigated by earlier workers^{13,59–61}.

In addition, within this structure there are significant weak $\pi\cdots\pi$ intermolecular interactions between the pyrimidine rings of (dmbpy) ligands from neighboring chains, which are almost parallel to each other, with a $\text{Cg1}\cdots\text{Cg2}$ and $\text{Cg2}\cdots\text{Cg2}$ distance of 3.761 (7) Å and 3.747(9) Å, respectively, Fig. 11.

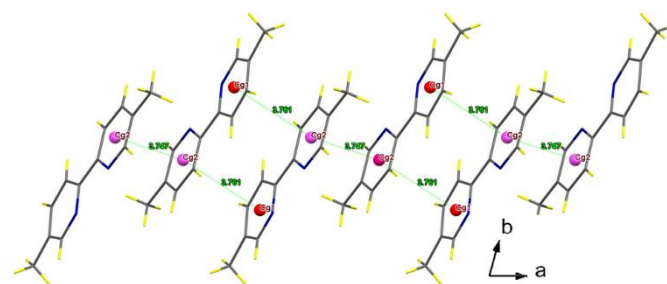


Fig. 11 View of the 1D supramolecular layered by intermolecular $\pi\cdots\pi$

Concurrently, C–H $\cdots\pi$ interactions were also observed between bridged CH₃-groups of the 5,5'-dimethyl-2,2'-bipyridine or the acetate molecules act as hydrogen bond donors towards the Cg of pyrimidine rings of (dmbpy) to form $\text{C12–H12B}\cdots\text{Cg1}$, $\text{C23–H23B}\cdots\text{Cg4}$, $\text{C28–H28A}\cdots\text{Cg4}$ and $\text{C30–H30A}\cdots\text{Cg4}$ interactions, with are distances 3.393, 3.176, 3.531 and 3.440 Å, respectively. $\pi\cdots\pi$ stacking and C–H $\cdots\pi$ interactions occur between the 1D chains along [100] direction. Further investigation of the packing structure showed that the assembly of the 0D of (2) into a 2D supramolecular architecture is also accomplished via C–H \cdots O hydrogen bonds, $\pi\cdots\pi$ and C–H $\cdots\pi$ involving the (dmbpy) and acetate ligands Fig. 12. The corresponding interactions of 2 are summarized in Table 3.

Table 3 Hydrogen bond, C–H $\cdots\pi$ and $\pi\cdots\pi$ stacking interactions in 2

D–H \cdots A ^{a,b}	D–H/Å	H \cdots A/Å	D \cdots A/Å	$\angle\text{D–H}\cdots\text{A}/^\circ$
$\text{C13–H13}\cdots\text{O1}$	0.93	2.41	2.918 (9)	114
$\text{C1–H1}\cdots\text{O2}$	0.93	2.39	2.914 (10)	115
$\text{C4–H4}\cdots\text{O4}^i$	0.93	2.50	3.385 (11)	158
$\text{C19–H19}\cdots\text{O7}^{ii}$	0.93	2.46	3.367 (13)	165
$\text{C30–H30C}\cdots\text{O7}$	0.96	2.66	3.499 (15)	146
$\text{C12–H12B}\cdots\text{Cg1}$	0.96	3.393	3.921	116
$\text{C23–H23B}\cdots\text{Cg4}$	0.96	3.176	3.936	137
$\text{C28–H28A}\cdots\text{Cg4}$	0.96	3.531	4.078	118
$\text{C30–H30A}\cdots\text{Cg4}$	0.96	3.440	4.282	147
^a Symmetry codes: (i) $-x+1, -y+2, -z+1$; (ii) $-x, -y+1, -z+2$.				
$\pi\cdots\pi$ interactions, Cg \cdots Cg distance/Å				
$\text{Cg1}\cdots\text{Cg2}^{iii}$	3.761(7)			
$\text{Cg2}\cdots\text{Cg2}^{iv}$	3.747(9)			
$\text{Cg3}\cdots\text{Cg3}^v$	3.654(8)			
^b Symmetry codes: (iii) $1-x, 2-y, 1-z$; (iv) $-x, 2-y, 1-z$; (v) $1-x, 1-y, 2-z$				
^b Cg1, Cg2, Cg3 and Cg4 are the centroids of the N1–C1–C2–C3–C4–C5, N2–C6–C7–C8–C9–C10, N3–C13–C14–C15–C16–C17, N4–C18–C19–C20–C21–C22.				

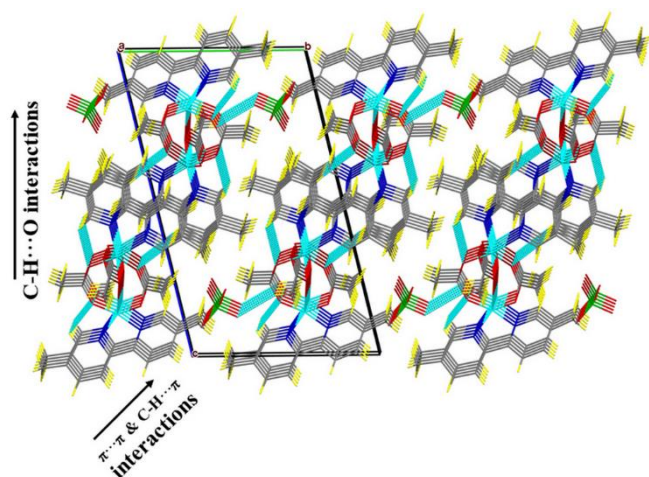


Fig. 12 3D supramolecular structure induced by intermolecular interactions in (2), view along *a*.

Hirshfeld surfaces

The Hirshfeld surfaces of two Ni(II) and Cu(II) compounds are illustrated in Fig. 13 showing the surfaces that have been mapped over d_{norm} (-0.32 to 1.56 Å), shape index (-1.0 to 1.0 Å) and curvedness (-4.0 to 0.4 Å). The surfaces are shown as transparent to allow visualization of molecules, in a similar orientation for all of the structures, around which they were calculated. We have considered the asymmetric unit among the entire unit cell for all of the compounds. It is clear that the information present in the hydrogen bonding tables is summarized effectively in these spots, with the large circular depressions deep red visible on the d_{norm} surfaces and is marked as (A) indicative of hydrogen bonding contacts (the oxygen atoms one near to groups CH₃COO⁻ and another on the perchlorate anions), and other light red spots labelled (B) are due to H...H contacts (π - π interactions). The small extent of area marked as (C) and light color on the surface indicates other weaker and longer contacts are due to H...C contacts (C-H... π interactions) (Figure 13a). Furthermore, the Hirshfeld surfaces were mapped with shape index and curvedness functions to evaluate the presence of C-H... π stacking interactions, which are clearly visible in the analysis of the crystal structure. In the shape index diagram of both compounds (Figure 13b), inspection of the adjacent red and blue triangles on the shape index surface shows the existence of π -stacking interactions in the structure of both compounds, involving the 2,2'-bipyridine ring. The interaction is almost identical in the two crystal structures. i.e. blue triangles represent convex regions due to ring carbon atoms of the molecule inside the surface, while red triangles represent concave regions due to carbon atoms of the 5,5'-dimethyl-2,2'-bipyridine stacked molecule above it. The curvedness mapped on the Hirshfeld surface (Fig. 13c) shows that the largest region of flat curvedness appears for compound 2. This analysis is conforming to the structural results. Indeed, in the crystal packing of both compounds, π - π interactions are clearly visible in the analysis of the section crystal structures, with Cg1...Cg2 distances of 3.775 for (1) and 3.761 Å for (2). These interactions are also noticeable as

relatively large and green flat regions delineated by the red circle on the curvedness surfaces of both compounds.

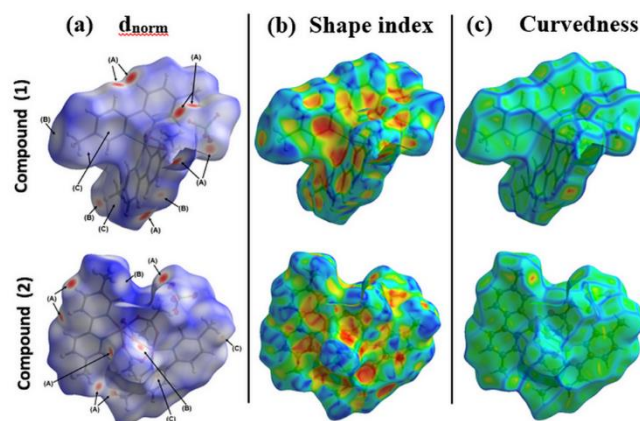


Fig. 13 Hirshfeld surfaces mapped with d_{norm} (a), shape index (b), and curvedness (c) for compounds 1 and 2.

The full 2D fingerprint plots of the main intermolecular interactions of the compounds Ni(II) and Cu(II) are depicted in Figure 14 and Figure S2. The comparison of the relative contributions of different interactions (Fig. 12) indicates the more or less identical contribution of interactions in these two Ni(II) and Cu(II) complexes due to their structural similarity. According to the Hirshfeld surface analysis, for all molecules of 1 as well as for 2, the intermolecular H...H contacts (H...H intermolecular contacts), are in the range from 44.4 to 44.8 % (Fig. 15) of the total number of contacts, which marks them as highly dominant contributors to the crystal packing. H...H interactions appeared as a very distinct spike on the diagonal of the plots. They have the lowest value of $d_e + d_i$ in both complexes (≈ 2.6 Å in (1) and 2.5 Å in (2)).

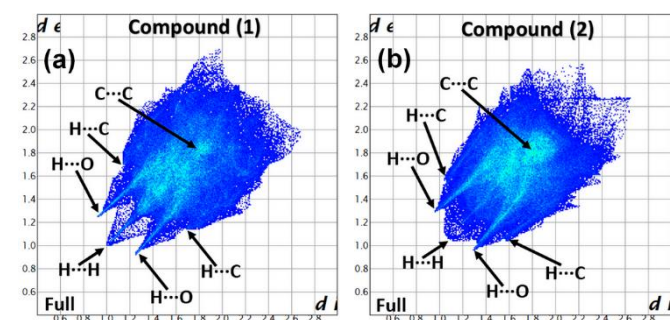


Fig. 14 Fingerprint plots for compounds 1 and 2.

The proportions of O...H/H...O interactions comprise 29.4% and 31.7% of the total Hirshfeld surface for each molecule of (1), and (2), respectively. The O...H interactions are represented by a spike ($d_i \approx 0.92$, $d_e \approx 1.27$ Å in Ni(II) and $d_i \approx 0.97$, $d_e \approx 1.31$ Å in Cu(II)) in the bottom left area of the fingerprint plot (Figure S2). The Hirshfeld surface analysis does not show a similar proportion of O...H interactions for each oxygen atoms of the perchlorate and acetate groups. In all cases, this result confirms that the carbon atoms of 5,5'-dimethyl-2,2'-bipyridine and acetate ligands are in contact with the oxygen atoms, leading to the formation of the ($R_2^2(12)$, $R_4^4(18)$

and $R_2^2(12)$, $R_4^4(20)$ ring motifs responsible for the formation of the 2D and 1D supramolecular self-assembly in 1 and 2, respectively. The structures of two Ni(II) and Cu(II) molecules are also dominated by H...C contacts, from 18.8 to 13.9% (Fig. S4) of the total Hirshfeld surface areas. These contacts in the corresponding fingerprint plots are shown in the form of “wings” with the shortest $d_e + d_i \approx 2.6$ – 2.7 Å. Moreover, also worth mentioning is the contribution of C...C contacts (associated with π ... π stacking interactions) contacts ranging from 3.7 to 4.8% in both structures (Fig. 15). They are shown on the fingerprint plots as a region of blue/flat green color on the diagonal around $d_e \approx d_i \approx 1.63$ Å and $d_e \approx d_i \approx 1.71$ Å for complexes (1) and (2), respectively, which are clearly visible in the analysis of the crystal structures, with Cg1...Cg2 distances of 3.775 for (1) and ranging from 3.654 to 3.761 Å for Cg3v...Cg3iv and Cg1...Cg2, respectively, for (2). Close inspections of the other intermolecular contacts also revealed a negligible proportion of H...N (2.1–2.6%), C...O (1.2–0.5%) and C...N (0.2–1.1%) contacts in the structures of all molecules of (1) and (2) (Fig. S4). All the above considerations are based on intramolecular distances and angles, it would be very interesting to convert those experimental parameters into true interaction energies; but the latter is still a challenge in molecular crystals though some results have been recently obtained on metal coordination complexes that are to some extent similar to the present ones.⁶²

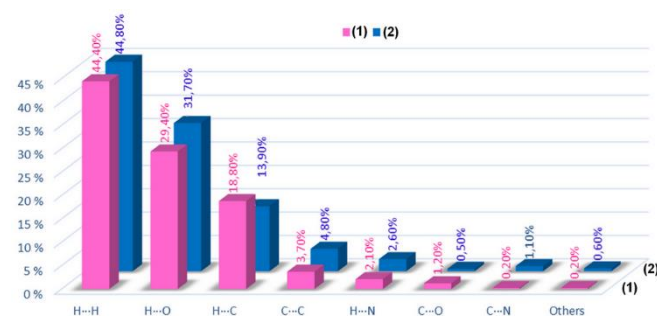


Fig. 15 Relative contributions of various intermolecular contacts to the Hirshfeld surface area in 1 and 2.

Optical properties

The UV-Vis absorption properties of (1) (d^8 , mononuclear) and (2) (d^9 , homobinuclear) have been examined in the solid state at room temperature. As shown in Fig. 16, (1) exhibits absorption peaks at 239 nm along with a broad absorption consisting of two peaks with the maximum at 498 nm. (2) features a new absorption at 398 nm except for two comparable absorptions at 235, and 693 nm but with a noticeable red-shift compared to (1). The first ones well resolved bands are assignable to intraligand transitions, $\pi \rightarrow \pi^*$ (LLCT) in (1) and (2). The intense band at 394 nm appear for copper(II) complex is primarily due to a ligand-metal charge transfer (MLCT) associated with the nitrogen and oxygen donors.^{63,64} In addition to these bands, in the visible region, bands are assigned to the d-d transitions of the metal ions, present in the title compounds. With this in mind, observed absorption peaks at 407–701 nm region for compound (1) can be attributed to d-d transitions with the modes of ${}^3A_{2g} \rightarrow {}^3T_{1g(P)}$ and ${}^3A_{2g} \rightarrow {}^3T_{1g(F)}$, which are well matched with the results observed

in other octahedral Ni(II) coordination compounds.^{65,66} In homobinuclear compound (2), relatively weak intensity the band in 701 nm characteristic of to the $d_{x^2-y^2} \rightarrow d_{z^2}$ as expected for distorted squar-pyramidal and distorted square-planer copper(II) complexes with confirming the $d_{x^2-y^2}$ based ground state and elongation of the axial bonds. Such types of absorption bands between Cu(II)–Cu(II) homobinuclear copper(II) complexes were observed in homobinuclear complexes reported in the literature.^{8,67-69}

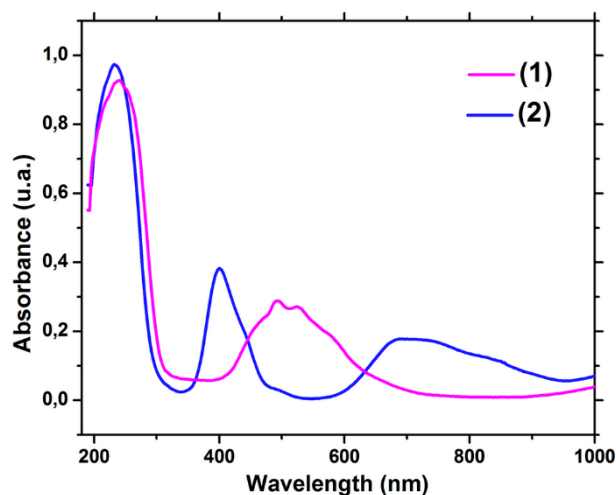


Fig. 16 UV-vis Absorption spectra of compounds 1 and 2.

The optical band gap energy was calculated according to the equation Tauc:

$$\alpha h\nu = A(h\nu - E_g)^n$$

where A is a constant, $h\nu$ is the incident photon energy, and E_g is the optical band gap material, n was considered to be equal to $\frac{1}{2}$ in the equation for calculating the band gap of the complexes.⁷⁰ For this compounds the gap energy is of direct type because the absorption band used for the energy calculation is located outside the visible range (239 nm in (1) and 235 nm in (2)).⁷¹ The band gap energy was estimated to be 4.17 eV and 4.32 eV for (1) and (2) respectively (Fig. 17), which falls in the UV region (< 3.1 eV for visible region). These values clearly classify these materials among the semiconductor materials.^{72,73}

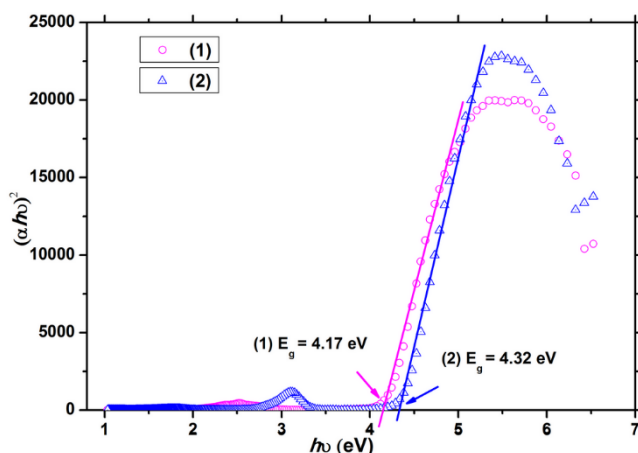


Fig. 17 Tauc plots analysis of compounds 1 and 2.

ARTICLE

Conclusions

In summary, both new complexes [Ni(dmbpy)₂(CH₃COO)]ClO₄ (1) and [Cu₂(dmbpy)₄(CH₃COO)₃]ClO₄ (2) were characterized by means of single-crystal X-ray diffraction, elemental analysis, IR spectroscopy, TGA/DTA and UV-Vis spectroscopy. Both compounds similarly crystallize in the triclinic system, with the centrosymmetric space group P-1. In each case, 5,5'-dimethyl-2,2-bipyridine molecules play the role of hydrogen bonding linkages between the acetate and perchlorate oxygen atoms in (1) and (2). In compound (1) the formation of multiple hydrogen bonding, C-H...π and π...π stacking interactions can act as primary tools for constructing 3D supramolecular architectures. For (2), C-H...O hydrogen bonds lead to the stacking of 1D (pseudo-)chains into a 2D network. Intermolecular interactions were visualized and quantified using Hirshfeld surfaces with two dimensional fingerprint plots. These analyses put in light the effective role of H...H, O...H, C-H...π and π...π contacts in the cohesion of the crystal packing of (1) and (2). The 2D fingerprint plots indicate the more or less identical contributions of interactions in the complexes arising from their structural similarity. The optical properties show that the samples have a semiconducting character.

Author Contributions

All authors contributed equally

Conflicts of interest

There are no conflicts to declare.

Acknowledgements

The authors thank the University of Sfax-Tunisia for financial support. The X-ray diffraction is performed at the XRD center of ICMCB.

Supplementary information

CCDC numbers of 2085397 and 2085398 are corresponded to the supplementary crystallographic data for this paper. These data are available free of charge at <http://www.ccdc.cam.ac.uk/conts/retrieving.html>.

Notes and references

- 1 T. A. Manz and B. Yanga, *RSC Adv.*, 2014, **4**, 27755-27774.
- 2 J. Hwang, A. Ejsmont, R. Freund, J. Goscianska, B. V. K. J. Schmidt and S. Wuttke, *Chem. Soc. Rev.*, 2020, **49**, 3348-3422.
- 3 Y.F. Han and G. X. Jin, *Acc. Chem. Res.*, 2014, **47**, 12, 3571-3579
- 4 M. A. Petrukhina, A. S. Filatov, Y. Sevryugina, K. W. Andreini and Takamizawa, *Organometallics*, 2006, **25**, 9, 2135-2142.
- 5 X.Qiao, Z.Y.Ma, C.Z. Xie, F. Xue, Y.W. Zhang, J.Y. Xu, Z.Y. Qiang, J.S. Lou, G.J. Chen and S.P. Yan, *J. Inorg. Biochem.*, 2011, **105**, 728-737.
- 6 I. Ahmed and S. H. Jung, *Chem. Eng. J.*, 2017, **310**, 197-215.
- 7 Q. X. Liu, Q. Wei, X.J. Zhao, H. Wang, S. J. Li and X. G. Wang, *Dalton Trans.*, 2013, **42**, 5902-5915.
- 8 Y. P. Singh, R. N. Patel, Y. Singh, D. Choquesillo-Lazarte and R. J. Butcher, *Dalton Trans.*, 2017, **46**, 2803-2820.
- 9 N. N. Adarsh, M. M. Dîrtu, P. Guionneau, E. Devlin, Y. Sanakis, J. A. K. Howard, B. Chattopadhyay and Y. Garcia, *Eur. J. Inorg. Chem.*, 2019, **5**, 585-591.
- 10 I.A. Golenya, E. Gumienna-Kontecka, M. Haukka, O. M. Korsun, O. N. Kalugin and I. O. Fritsky, *Dalton Trans.*, 2017, **46**, 2803-2820.
- 11 S. P. Yelgaonkar, D. Kiani, J. Baltrusaitis and L. R. MacGillivray, *Chem. Commun.*, 2020, **56**, 6708-6710.
- 12 S. K. Seth, A. Bauzá and A. Frontera, *CrystEngComm*, 2018, **20**, 746-754.
- 13 P. Manna, S. K. Seth, A. Das, J. Hemming, R. Prendergast, M. Helliwell, S. R. Choudhury, A. Frontera, and S. Mukhopadhyay, *Inorg. Chem.*, 2012, **51**, 3557-3571.
- 14 T. H. Huang, S. L. Zhu, X.L. Xiong, J. D. Li, H. Yang, X. Huang, X. R. Huang and K. Zhang, *J. Mol. Struct.*, 2017, **1143**, 431-437.
- 15 M. Montazerzohori, A. Masoudiasl, Th. Doert and H. Seykens, *RSC Adv.*, 2016, **6**, 21396-21412.
- 16 S. T. Salammal, Z. Zhang, J. Chen, B. Chattopadhyay, J. Wu, Lei Fu, C. Fan, and H. Chen, *ACS Appl. Mater. Interfaces*, 2016, **8**, 32, 20916-20927.
- 17 L. S. Xie, E. V. Alexandrov, G. Skorupskii, D. M. Proserpio and M. Dinca, *Chem. Sci.*, 2019, **10**, 8558-8565.
- 18 L. Liu, J. Hao, Y. Shi, J. Qiu and C. Hao, *RSC Adv.*, 2015, **5**, 3045-3053.
- 19 M. Zeng and Y. Zhang, *Chem. Sci.*, 2019, **10**, 8558-8565.
- 20 B. Chen, Z.-P. Lv, C. F. Leong, Y. Zhao, D. M. D'Alessandro and J.-L. Zuo, *Cryst. Growth Des.*, 2015, **15**, 1861-1870
- 21 J. P. Pouget, P. Alemany and E. Canadell, *Mater. Horiz.*, 2018, **5**, 590-640.
- 22 J. Yoshida, A. Ueda, R. Kumai, Y. Murakami and H. Mori, *CrystEngComm*, 2017, **19**, 367-375.
- 23 S. S. Massoud, F. R. Louka, F. A. Mautner, *CrystEngComm*, 2015, **17**, 7604-7617.
- 24 A. Heuer-Jungemann, N. Feliu, I. Bakaimi, M. Hamaly, A. Alkilany, I. Chakraborty, A. Masood, M. F. Casula, A. Kostopoulou, E. Oh, K. Susumu, M. H. Stewart, I. L. Medintz, E.I Stratakis, W. J. Parak, and A. G. Kanaras, *Chem. Rev.*, 2019, **119**, 8, 4819-4880.
- 25 Z.H. Zhu, H.L. Wang, H.H. Zou, and F.P. Liang, *Dalton Trans.*, 2020, **49**, 10708-10723.
- 26 Y. Navarro, G. P. Guedes, J. Cano, P. Ocón, M. J. Iglesias, F. Lloret and F. López-Ortiz, *Dalton Trans.*, 2020, **49**, 6280-6294
- 27 R. Jaballi, W. Maalej, D. Atoui, H. Feki, R. Ben Salem and Z. Elaoud, *Appl. Organomet. Chem.*, 2018, **32**, 34, e4366.
- 28 G. Mouchaham, N. Roques, A. Kaiba, P. Guionneau and J. Sutte, *CrystEngComm*, 2010, **12**, 3496-3498.
- 29 W. Maalej, P. Guionneau and Z. Elaoud, *J. Mol. Struct.*, 2021, <https://doi.org/10.1016/j.molstruc.2021.130630>.
- 30 X. Ding, S. Wang, Y. Lia and W.Huang, *Inorg. Chem. Front.*, 2015, **2**, 263-272.
- 31 L.Long, *CrystEngComm*, 2010, **12**, 1354-1365.
- 32 S. Zhang, F. Jiang, M. Wu, Lian Chen, J.Luo and M. Hong, *CrystEngComm*, 2013, **15**, 3992-4002.
- 33 R.Jaballi , D. Atoui, W. Maalej, A. Babaryk, P. Horcajada, R. B. Salem, and Z. Elaoud, *J. Mol. Struct.*, 2020, **1219**, 128572.
- 34 M. Wojtaś, V. Kinzhyballo, I. Bdikin and A. L. Kholkin, *Cryst. Growth Des.*, 2019, **19**, 2583-2593.
- 35 H. Keypour, M. Shayesteh, S. Salehzadeh, S. Dhers, F. Maleki, H. Unverc and N. Dilek, *New J. Chem.*, 2015, **39**, 7429-7441.
- 36 T. S. Mahapatra, S. Chaudhury, S. Dasgupta, V. Bertolasi, and D. Ray, *New J. Chem.*, 2016, **40**, 2268-2279.
- 37 A. B. Rached, W. Maalej, P. Guionneau , N. Daro , T. Mhiri , H. Feki and Z. Elaoud, *J. Phys. Chem. Solids*, 2018, **123**, 150-156.

- 38 K. Rodpun, A. G. Blackman, M. G. Gardiner, E. W. Tan, C. J. Meledandri and N. T. Lucas, *CrystEngComm*, 2015, **17**, 2974-2988.
- 39 K. Ghosh, P. Kumar, N. Tyagi, U. P. Singh, V. Aggarwal and M. C. Baratto, *Eur. J. Med. Chem.*, 2010, **45**, 3770-3779.
- 40 B. J. Hathaway and A. E. Underhill, *J. Chem. Soc.*, 1961, 3091-3096.
- 41 S. S. Massoud, T. Junk, F. R. Louka, R. Herchel, Z. Travnicek, R. C. Fischer and F. A. Mautner, *RSC Adv.*, 2015, **5**, 87139-87150.
- 42 A. W. Herlinger, S. L. Wenhold, T. V. Long, *J. Am. Chem. Soc.*, 1970, **92**, 22, 6474-6481.
- 43 N. F. Curtis and Y. M. Curtis, *Inorg. Chem.*, 1965, **4**, 804-809.
- 44 G. Sheldrick, Crystal structure refinement with SHELXL, *Acta Cryst. C*, 2015, **C71**, 3-8.
- 45 L. J. Farrugia, WinGX and ORTEP for Windows: an update, *J. Appl. Crystallogr.*, 2012, **45**, 849-854.
- 46 E. Tailleux, M. Marchivie, N. Daro, G. Chastanet, P. Guionneau, *Chem. Commun.* 2017, **53**, 4763-4766.
- 47 E. Collet and P. Guionneau, *Comptes Rendus Chimie*, 2018, **21**, 1133-1151
- 48 F. L. Hirshfeld, *Theoret. Chim. Acta*, 1977, **44**, 129-138.
- 49 J. J. McKinnon, D. Jayatilaka and M. A. Spackman, *Chem. Commun.*, 2007, **37**, 3814-3816.
- 50 A. Parkin, G. Barr, W. Dong, C. J. Gilmore, D. Jayatilaka, J. J. McKinnon, M. A. Spackman and C. C. Wilson, *CrystEngComm*, 2007, **9**, 648-652.
- 51 A. L. Rohl, M. Moret, W. Kaminsky, K. Claborn, J. J. McKinnon and B. Kah, *Cryst. Growth Des.*, 2008, **8**, 12, 4517-4525.
- 52 J. Bernstein, R. E. Davis, L. Shimon, and N. Chang, *Angew. Chem. Int. Ed. Engl.*, 1995, **34**, 1555-1573.
- 53 J. A. Platts, S. T. Howard and K. Woźniak, *Chem. Phys. Lett.*, 1995, **232**, 479-485.
- 54 H. Li, N. Ma and K. Li, *J. Inorg. Organomet. Polym. Mater*, 2012, **22**, 1320-1324.
- 55 A. Sarkar, A. R. Paital, R. A. Khan, F. Arjmand, V. Bertolasi, C. Mathonière, R. Clérac, and D. Ray, *Dalton Trans.*, 2013, **42**, 12495-12506.
- 56 A. W. Addison, T. N. Rao, J. Reedijk, J. van Rijn and G. C. Verschoor, *J. Chem. Soc., Dalton Trans.*, 1984, **7**, 1349-1356.
- 57 A. S. Degtyarenko, M. Handke, K. W. Krämer, S. Liu, S. Decurtins, E. B. Rusanov, L. K. Thompson, H. Krautscheid and K. V. Domasevitch, *Dalton Trans.*, 2014, **43**, 8530-8542.
- 58 F. Sama, A. K. Dhara, M. N. Akhtar, Y. Chen, M. L. Tong, I. A. Ansari, M. Raizada, M. Ahmad, M. Shahid and Z. A. Siddiqi, *Dalton Trans.*, 2017, **46**, 9801-9823.
- 59 C. D. A. León, G. A. Echeverría, O. E. Piro, S. E. Ulic, J. L. Jios, J. A. Pereañez, I. C. H. Castañeda, H. Pérez, *New J. Chem.*, 2017, **41**, 14659-14674.
- 60 A. Wu and K. Lee, *CrystEngComm*, 2012, **14**, 3424-3432.
- 61 C. Lee, F. Su, Y. Lin, C. Chou and K. Lee, *CrystEngComm*, 2011, **13**, 2318-2323.
- 62 M. Reeves, E. Tailleux, P. Wood, M. Marchivie, G. Chastanet, P. Guionneau, and S. Parsons, *Chem. Sci.*, 2021, **12**, 1007-1015.
- 63 R. Cao, Q. Sun, D. Sun, M. Hong, W. Bi and Y. Zhao, *Inorg. Chem.*, 2002, **41**, 6161-6168.
- 64 T. M. Donlevy, L. R. Gahan, T. W. Hambley, G. R. Hanson, K. L. McMahon and R. Stranger, *Inorg. Chem.*, 1994, **33**, 5131-5137.
- 65 Z. Wang, Z. Jagličić, L. Han, G. Zhuang, G. Luo, S. Zeng, C. Tung and D. Sun, *CrystEngComm*, 2016, **18**, 3462-3471.
- 66 B. K. Das, S. J. Bora, M. Chakraborty, L. Kalita, R. Chakraborty and R. Barman, *J Chem Sci*, 2006, **118**, 487-494.
- 67 I. M. Procter, B. J. Hathaway, D. E. Billing, R. Dudley and P. Nicholls, *J. Chem. Soc. A*, 1969, 1192-1197.
- 68 B. J. Hathaway and D. E. Billing, *Coord. Chem. Rev.*, 1970, **5**, 143-207.
- 69 D. Ghosh, N. Kundu, G. Maity, K. Choi, A. Caneschi, A. Endo, and M. Chaudhury, *Inorg. Chem.*, 2004, **43**, 19, 6015-6023.
- 70 J. Tauc, R. Grigorov, A. Vancu, *Phys. Status Solidi B* 15, 1966, **15** (2), 627-637.
- 71 M. Li, L. Kou, L. Diao, Q. Zhang, Z. Li, Q. Wu, W. Lu, D. Pan, and Z. Wei, *J. Phys. Chem. C*, 2015, **119**, 18, 9782-9790.
- 72 A. El-Korashy, H. El-Zahed, M. Radwan, *Physica B: Condensed Matter*, 2003, **334**, 75-81.
- 73 I. Dakhlaoui, K. Karoui, F. Hajaloui, F. Jomni, *Appl. Organomet. Chem.*, 2020, **34**, e5990.